Available online at www.sciencedirect.com
ScienceDirect
Engineering Structures 29 (2007) 1025–1033
ENGINEERING STRUCTURES
www.elsevier.com/locate/engstruct

# A study of tensile damage and attenuation effect of perforated concrete defense layer on stress waves

Zhi-liang Wang[a,*], Yong-chi Li[a], J.G. Wang[b], R.F. Shen[c]

[a] *Department of Modern Mechanics, University of Science and Technology of China, Hefei city, Anhui 230027, China*
[b] *Centre for Protective Technology, National University of Singapore, 10 Kent Ridge Crescent, Singapore 119260, Singapore*
[c] *Centre for Soft Ground Engineering, Department of Civil Engineering, National University of Singapore, Singapore 117576, Singapore*

Received 2 February 2006; received in revised form 10 June 2006; accepted 17 July 2006
Available online 25 September 2006

**Abstract**

Civil defense shelters are often constructed beneath the ground to provide protection against blast loadings. Concrete is widely used as the material for the defense layer of the shelters. This paper adopts a continuum damage model of brittle media to numerically investigate the dynamic fracture and attenuation effect of perforated concrete defense layer on stress waves from planar charge. The model includes damage accumulation and loading rate-dependence, and has been succinctly implemented into the dynamic finite element code, LS-DYNA, via its user defined subroutine. The numerical results reveal that the adopted model can well predict the tensile damage owing to the reflection of pressure waves from cavities and free boundaries. Again, the elastoplastic properties of concrete play significant roles in the stress-wave attenuation and the peak values of hydrostatic pressure beneath a circular cavity are largely reduced. One empirical formula is finally proposed to relate the decay factor of peak hydrostatic pressure to the cavity dimensions and relative position.


*Keywords:* Concrete defense layer; Cavity; Stress waves; Tensile damage; Attenuation effect; Decay factor; Empirical formula

## 1. Introduction

The diffraction and attenuation of stress-waves are important aspects in the design of civil defense shelters [18,4,22,16]. The development of modern military technology greatly enhances the destructive power and hit rate of new weapons, thus posing great challenges to defense engineering nowadays. Civil defense shelters are widely constructed beneath the ground to provide protection against blast loadings [18,1]. Blast waves due to planar charge detonation evolve into the propagation of stress-waves in underground media. Such waves will be diffracted when hitting obstacles such as cavity, crevice or other media. The wave stress intensity may be greatly reduced beneath these obstacles. This reduction of stress from the peak value is often termed as attenuation or insulation of stress-waves [16].

Civil defense shields are widely used to reduce or even prevent the damage and destruction of underground structures from blast or impact loading [17,9,11,22,3]. When designing a civil defense work, the attenuation of and screening against stress-waves must be considered and new stress-wave migration systems are expected. Some experimental tests related to this problem have been performed by the authors, and some field observations have been conducted. Fig. 1 is the full-scale test appearance, and Fig. 2 depicts the configuration of the experimental defense structure. It clearly shows that a layered defense structure typically consists of three layers [18,12]: a soil cover layer, a protection layer and a support layer. Furthermore, the protection layer has two sub-layers: a projectile shelter layer and a stress distribution layer. Generally speaking, the stress distribution layer is made of perforated concrete or buffer materials such as sand and geofoam. Its major function is to redistribute the blast loading over a larger area. However, studies on the function of the stress distribution layer are limited so far.

Artificial cavities are normally incorporated into the stress distribution layer to dissipate the energy of stress waves. The stress-wave attenuation due to the dynamic fracture and plastic deformation of the perforated concrete is far from well

* Corresponding author. Fax: +86 551 3606459.
*E-mail address:* GeowzL@yahoo.com.cn (Z.-l. Wang).

0141-0296/$ - see front matter © 2006 Elsevier Ltd. All rights reserved.
doi:10.1016/j.engstruct.2006.07.010

Fig. 1. Appearance of the field test for defense structure under planar charge.

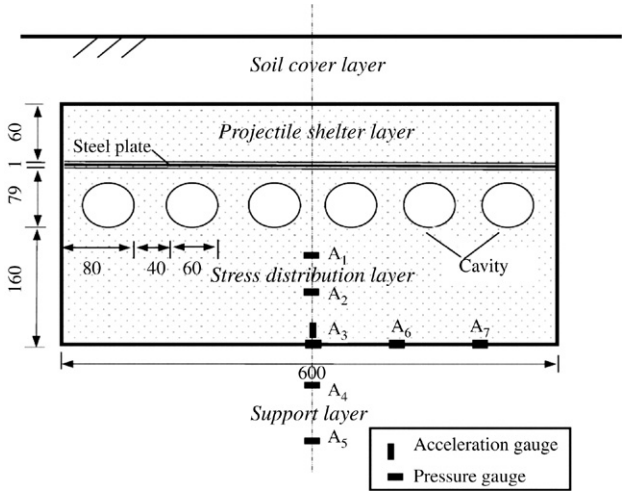


Fig. 2. Schematic of the defense structure in the test (unit in cm).

understood [19,20]. What is more, the existence of cavities in a perforated defense layer may create great potential of tensile damage above cavities due to the lower wave impedance of air inside the cavities. Besides, the potential damages due to reflected tensile waves near free boundaries (non-transmissive) should also receive attention. So far, studies on such phenomena are rarely found in literature.

In the present study, a continuum damage model for brittle media [21,13] is adopted and successfully implemented into the finite element software, LS-DYNA, through its user subroutine capability [14]. The numerical scheme with the model parameters are then calibrated against limited field test data. The tensile damage owing to the cavity and free boundary reflection is investigated subsequently. The attenuation effect of a single circular cavity on peak hydrostatic pressure is also explored in detail based on the damage model. Finally, an empirical formula is proposed to relate the decay factor for peak hydrostatic pressure to the cavity parameters.

## 2. Continuum damage model for concrete medium

Within a concrete mass, flaws and cracks exist even prior to any loading. Under externally tensile stresses, these flaws or cracks will grow in size and number, causing the deterioration of concrete stiffness and strength. In this section, a continuum damage model for brittle concrete was adopted and a software subroutine was specially developed for the study of the tensile damage and attenuation effects of perforated concrete defense layer on stress waves.

To make a complex problem more tractable, it is assumed that the concrete is an isotropic, homogeneous, continuous and brittle material with pre-existing micro cracks. The finite element program coupled with the defined model captures the general effects of the microcrack system on material stiffness, instead of treating individual cracks which are direction-sensitive. As for the damage process, it is assumed that damage is caused by the activation and growth of pre-existing microcracks. It is accumulated over time and is irreversible.

According to the concepts of continuum mechanics, for isotropic materials, when a material point is subjected to stresses, it changes in volume due to the volumetric parts of the stresses and in shape due to its deviatoric parts. The volumetric strain $\varepsilon_v$ is regarded as a time-dependent variable, which determines whether the microcracks will be activated and will evolve.

Under external loadings, the dynamic fracture of concrete does not occur unless the stress is larger than its tensile strength. This is accounted for by setting a critical value $\varepsilon_c$ for the volumetric strain $\varepsilon_v$ [15,13]:

$$\varepsilon_c = \frac{1-2v}{E}\sigma_s \tag{1}$$

where $E$ is the Young's modulus, $v$ is the Poisson's ratio and $\sigma_s$ represents the tensile strength of concrete.

Obviously, microcracks will be activated when $\varepsilon_v$ exceeds $\varepsilon_c$, whereas the microcrack system remains stable when $\varepsilon_v$ is less than $\varepsilon_c$. On the other hand, the concrete material will not fail if the duration of an applied stress whose value is well above the tensile strength is too short. In this regard, a crack density $C_d$ is defined as [21,13]:

$$C_d = \alpha(\varepsilon_v - \varepsilon_c)^\beta t \tag{2}$$

where $\alpha$ and $\beta$ are material constants, $t$ is time.

The differential form for the crack density is written as:

$$\mathrm{d}C_d = \alpha\beta(\varepsilon - \varepsilon_c)^{\beta-1} t\,\mathrm{d}\varepsilon_v + \alpha(\varepsilon_v - \varepsilon_c)^\beta \mathrm{d}t. \tag{3}$$

In the present model, the damage scalar $D$ is assumed to take the following form:

$$D = 1 - \exp(-C_d^2). \tag{4}$$

The degraded Young's modulus $E_d$ for the damaged concrete is computed as:

$$E_d = E \cdot (1 - D). \tag{5}$$

According to Jaeger and Cook [8], if a brittle body (rock, concrete) contains closed cracks, the effective Poisson's ratio is greater than its intrinsic Poisson's ratio. However, when the body contains very flat, open cracks or equidimensional cavities, the effective Poisson's ratio is smaller than its intrinsic Poisson's ratio. By assuming that all types of cracks are

generated equally during blast damage, the Poisson's ratio can be assumed to remain unchanged for the damaged body. The use of an unchanged Poisson's ratio also has the advantage that relationships among elastic parameters would not change for the damaged body [21].

As for a concrete mass, when it is under tension and $\varepsilon_v$ exceeds $\varepsilon_c$, the incremental relations for stress–strain is:

$$\Delta\sigma_{ij} = K_d\delta_{ij}\Delta\varepsilon_{kk} + 2G_d\Delta e_{ij} \tag{6}$$

where $K_d$ and $G_d$ are, respectively, the degraded bulk and shear moduli, $\delta_{ij}$ is the Kronecker delta, $\Delta\sigma_{ij}$ is stress increment, $\Delta\varepsilon_{kk}$ and $\Delta e_{ij}$ are increments of volumetric and deviatoric strains, respectively.

When total volumetric strains are less than the critical volumetric strain, elasto-plastic model is used to model the stress–strain properties of concrete and the Von Mises yield criterion with kinematic hardening is used for the plasticity model [15]. In this situation, elastic parameters of the undamaged concrete are adopted since it is assumed that micro cracks remain closed.

The yield condition [6] is expressed as:

$$\varphi = \Lambda^2 - \sigma_y^2 \tag{7}$$

where $\Lambda = \sqrt{\frac{3}{2}(s_{ij}-\omega_{ij})(s_{ij}-\omega_{ij})}$, $\sigma_y$ denotes the current radius of yield surface, and deviatoric stress $s_{ij}$ is calculated as:

$$s_{ij} = \sigma_{ij} - \frac{1}{3}\sigma_{kk}\delta_{ij}. \tag{8}$$

The center of the yield surface in deviatoric stress space is denoted by a moving tensor $\boldsymbol{\omega}$, whose initial value is zero, as follows:

$$\Delta\omega_{ij} = \frac{2}{3}(1-\psi)E_p\dot{\varepsilon}^p_{ij}\Delta t \tag{9}$$

where $\psi$ is the hardening parameter (zero for the kinematic case), $\Delta t$ denotes the time step, $E_p$ is the plastic hardening modulus, the current radius of yield surface $\sigma_y$ is the sum of initial yield strength $\sigma_0$ and the growth $\psi E_p\varepsilon^p_{\text{eff}}$:

$$\sigma_y = \sigma_0 + \psi E_p\varepsilon^p_{\text{eff}} \tag{10}$$

where the effective plastic strain $\varepsilon^p_{\text{eff}}$ is defined by:

$$\varepsilon^p_{\text{eff}} = \int_0^t \sqrt{\frac{2}{3}\dot{\varepsilon}^p_{ij}\dot{\varepsilon}^p_{ij}}\,\mathrm{d}t. \tag{11}$$

The plastic strain ratio is the difference between total and elastic strain (right superscript $e$) ratios:

$$\dot{\varepsilon}^p_{ij} = \dot{\varepsilon}_{ij} - \dot{\varepsilon}^e_{ij}. \tag{12}$$

In Eq. (7), $\varphi \le 0$ is for elastic or neutral loading while $\varphi > 0$ is for plastic hardening. The effective plastic strain $\varepsilon^p_{\text{eff}}$ and stress tensors $\sigma_{ij}$ at time $t_{n+1}$ respectively are as follows:

$$(\varepsilon^p_{\text{eff}})^{n+1} = (\varepsilon^p_{\text{eff}})^n + \Delta\varepsilon^p_{\text{eff}} \tag{13}$$

$$\sigma^{n+1}_{ij} = S^{n+1}_{ij} + p^{n+1}\delta_{ij} \tag{14}$$

where,

$$S^{n+1}_{ij} = S^*_{ij} - \sqrt{6}G\Delta\varepsilon^p_{\text{eff}} \tag{15}$$

$$\Delta\varepsilon^p_{\text{eff}} = \frac{\Lambda - \sigma^n_y}{3G + E_p} \tag{16}$$

in which, $\sigma^n_y$ is the yield limit at time $t_n$, $S^*_{ij}$ and $p^{n+1}$ represent the elastic deviatoric stress state and the hydrostatic pressure at time $t_{n+1}$.

## 3. Establishment and calibration of numerical scheme

### 3.1. Numerical tool

In the present study, the authors have successfully implemented the continuum damage concrete model described above into the software package, LS-DYNA, as a constitutive augment. This LS-DYNA software from the *Livermore Software Technology Corporation* can handle either two- or three-dimensional problems for high-speed impact and explosion [6,14].

### 3.2. Determination of model parameters

As is known, concrete C30 is usually used to construct the protection layer in civil defense engineering. The typical physical parameters are as follows: initial density $\rho_0 = 2240.0\ \text{kg/m}^3$, the Young's modulus $E = 30.0$ GPa, the Poisson's ration $v = 0.18$, uniaxial compression strength $\sigma_c = 30.0$ MPa. Assuming the tensile strength to be one-tenth of the uniaxial compression strength, the critical volumetric strain $\varepsilon_c$ ($=6.4\times10^{-5}$) can be calculated using Eq. (1).

In the continuum damage constitutive model, a critical parameter is the crack density as defined by Eq. (2), which in turn is greatly influenced by the parameters $\alpha$ and $\beta$. Thereinto, $\beta$ is the material constant which determines the rate-dependence of fracture stress. It has been observed by many researchers that the fracture stress for most brittle materials like rock and concrete depends on the cube root of the strain rate and can be taken as 2.0 [13,21]. So far, not much experience is available on the evaluation of the parameter $\alpha$ which should normally be determined by test data (see, for example, [13]). In view of this and with the aim to validate the developed numerical subroutine for the continuum damage constitutive model, a field blast test is conducted in the present study [12]. In the test, planar charge is adopted as shown in Fig. 3 which gives the arrangement of the blasting fuses in the shallow ground level. Since the rise time of blast loading is typically very short and the overpressure decays exponentially after the peak value, an equivalent triangular pressure pulse (see Fig. 4) is used to approximate the blast loading which is applied on the projectile shelter layer [2,5,20]. The intensity and duration of this overpressure depend on the explosive charge weight and the stand-off distance which usually follow the cubic laws [10, 2]. In the present study, the peak value $Q_{\max}$ is taken as about 120.0 MPa and occurs at time $t_{\max} = 0.0$ μs (micro second). This peak overpressure then decreases linearly to zero at time $t_c = 100.0$ μs.

Fig. 3. Field assembly of blasting fuses for planar charge.

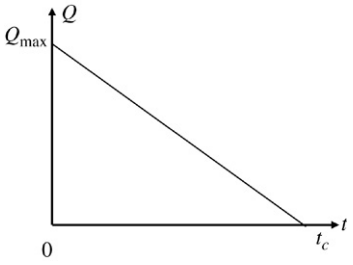


Fig. 4. Triangular impulse loading for explosion.

The subsurface configuration has been shown in Fig. 2 earlier, which also serves as the domain of finite element simulations. The FE simulations feature 4020 quadrilateral elements, inclusive of the steel plate (see Fig. 2) which is divided into 180 elements with the properties listed in Table 1. It is calibrated that, when $\alpha$ is taken to be $8.5\times10^{10}$, the numerical results are in fairly good agreement with the field recorded data. For example, Fig. 5 is the history of hydrostatic pressure at the stress gauge $A_2$ (refer to Fig. 2) which is on the symmetry axis and 159.0 cm below the lower surface of the steel plate. It is clear that the numerical simulations using the FE code

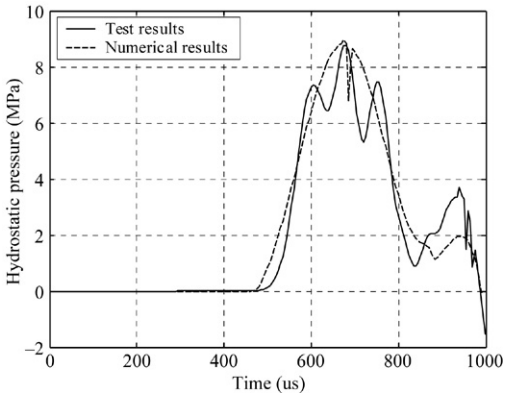


Fig. 5. Comparison of hydrostatic pressure between the numerical calculations and the field data from stress gauge $A_2$.

Table 1
Material parameters for steel plate used

| $\rho_0$ (kg/m$^3$) | $E$ (GPa) | $v$ | $\sigma_y$ (MPa) | $E_t$ (GPa) |
|---|---|---|---|---|
| 7900.0 | 207.0 | 0.29 | 274.0 | 2.1 |

LS-DYNA with the continuum damage model match favorably with the field measured data. The FEM simulation also reveals tensile damage at $t = 1000.0$ μs near the roof above the cavities as shown in Fig. 6. Such numerical revelation is corroborated by the post-blast field observation of the multiple tensile cracks on the roof layer as shown in Fig. 7. It should be noted that due to the very limited field data available, more extensive comparison of numerical predictions and field test data is not available. Details of the field blast test can be referred to in [12].

## 4. Numerical investigations

### 4.1. Definition of decay factor

The established numerical scheme encompassing the developed user subroutine of the continuum damage model was used for further investigations on the attenuation effects

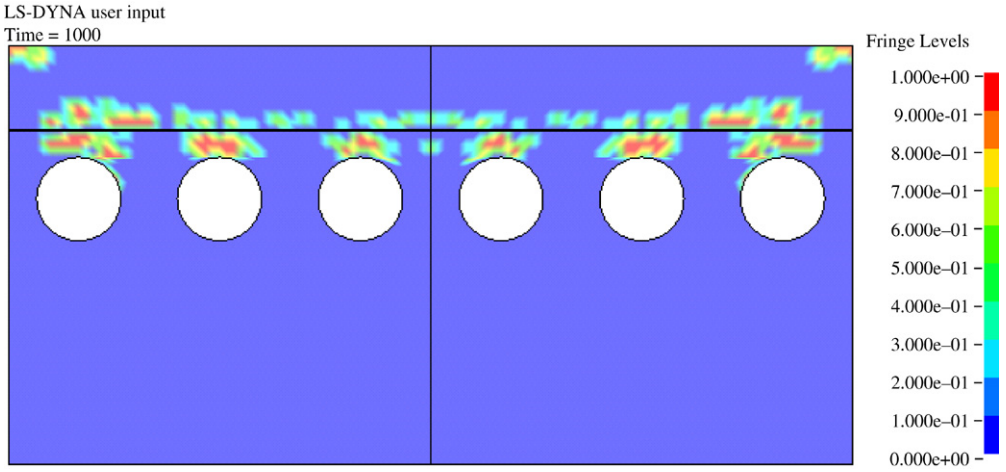


Fig. 6. Contours of tensile damage in problem domain.

Fig. 7. Post-blast tensile damage of a roof of one projectile shelter layer.

of concrete defense layer on blast stress-waves in the case of single cavity. To evaluate the attenuation extent of stress-waves due to a cavity in an intelligent defense layer, a dimensionless variable, 'decay factor' $DF$, is defined as follows:

$$DF = \frac{\sigma_0 - \sigma}{\sigma_0} \tag{17}$$

where $\sigma_0$ denotes the peak value of stress component such as $\sigma_x$, $\sigma_y$, or $P$ at a specified position without cavity in the defense layer, and $\sigma$ is the peak value of the same component at the same position with a cavity in the defense layer. Eq. (17) reveals that a larger $DF$ would imply a superior attenuation effect.

### 4.2. Computational domain with cavity

Fig. 8 shows the simulation of stress distribution layer embedded with a single circular cavity. The computational domain for this two-dimensional model is taken as 600 cm × 300 cm (width × height). The upper apex of the cavity is at a depth $e$ beneath the surface and the circular cavity has a radius $R$. Thus the coordinates of the center is $(0, e + R)$. Other dimensions are labeled in Fig. 8. Introducing the term relative distance $y$ as the distance between point $A$ and the lower apex of the cavity, the dimension $Y$ follows the following relationship:

$$Y = y + 2R + e. \tag{18}$$

Only the right half of the domain is selected in the computations owing to symmetry. As shown in Fig. 8, the right domain has the following boundary conditions: pressure boundary on the top, non-transmission boundaries (free reflection) on the right and lower sides, and symmetric boundary on the left side.

### 4.3. Effect of cavity size

Five radii are chosen in the computations: 0.0, 0.15, 0.30, 0.45 and 0.60 m, respectively. The parameter $e$ is fixed as 0.30 m. The model parameters for concrete are the same as stated in Section 3. For comparison purpose, computations are also carried out using the primitive linear elastic (L-E) model of concrete. The variations of peak hydrostatic pressure $P$ with relative distance $y$ (refer to definition in Fig. 8) are

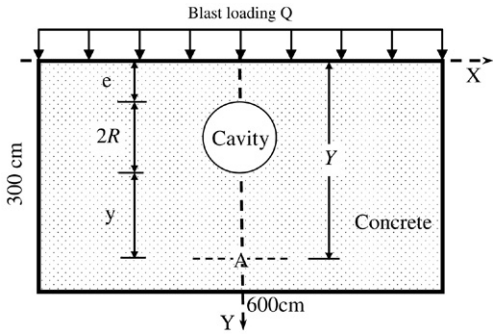


Fig. 8. Schematic of stress distribution layer with a single cavity.

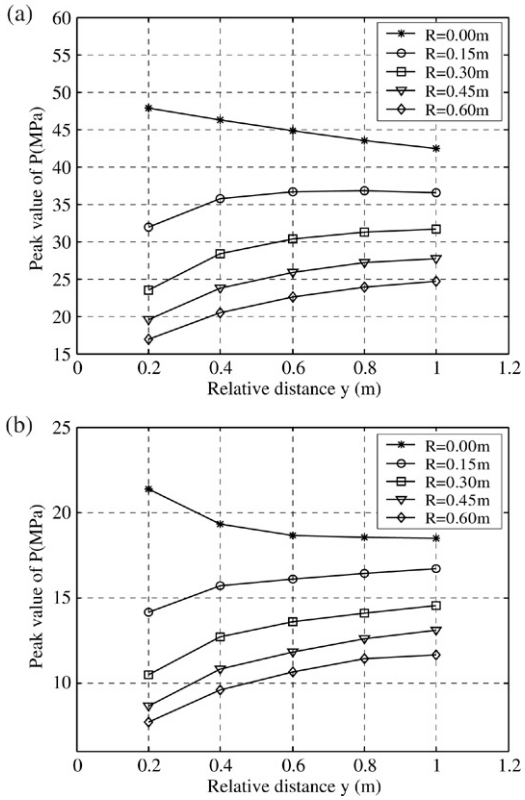


Fig. 9. Effect of different radii $R$ of circular cavity on peak hydrostatic pressure for (a) L-E model; and (b) continuum damage model.

shown in Fig. 9(a) for the L-E model and Fig. 9(b) for the continuum damage model. In both cases, the peak $P$ decreases with increasing radius $R$ for a specified position $y$. These results reveal that a larger cavity is more efficient in dissipating the wave energy. On the other hand, the peak $P$ increases with relative distance $y$ for a nonzero $R$, which indicates that wave energy experiences the maximum attenuation around the lower apex of the cavity and less attenuation further down below the cavity. Comparing the magnitudes of the peak $P$ in Fig. 9(a) and (b), it can be seen that the elastoplastic properties of concrete plays a crucial role on the magnitude of peak $P$. For instance, when $R = 0.30$ m and $y = 0.60$ m, the peak $P$ is 30.4 MPa for the L-E model and only 13.6 MPa for the damage model. The change of decay factor $DF$ with $R$ is shown in Fig. 10 for the

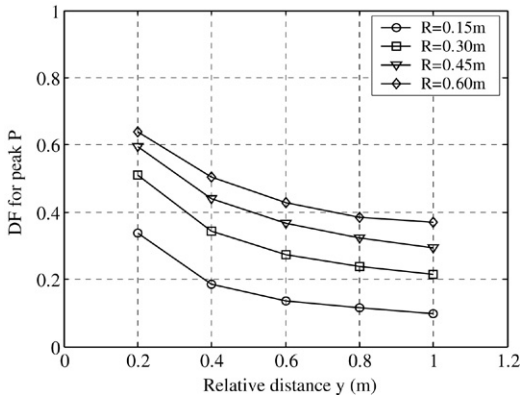


Fig. 10. Variation of decay factors for peak $P$ with different radii $R$ of cavity for continuum damage model.

damage model. It clearly shows that $DF$ increases with $R$ but reduces with increasing relative distance $y$.

Fig. 9 also shows that the curves for the case of zero $R$ (*i.e.* without cavity) are located at the highest positions of the plots, which demonstrates the effectiveness of a cavity in the attenuation of stress waves. The hydrostatic pressure contours for cases with and without cavity are further demonstrated in Fig. 11. Fig. 11(a) shows that the stress-waves are greatly disrupted due to the presence of the cavity. A tensile stress region is observed above the cavity, with a maximum value of almost 4.6 MPa. For a concrete grade C30, such large tensile stress would obviously exceed its tensile strength and lead to the tensile damage on the roof above the cavity. A zero-stress region can be noted in the adjacent domain beneath the cavity. The peak $P$ beneath the cavity is evidently lower. In addition, the reflected tensile waves can also be observed near the left and right boundaries. For the non-cavity case shown in Fig. 11(b), the tensile stress zone is only located at the side boundaries of the calculation domain and the continuity of wave front is hardly interrupted.

Fig. 12 compares the damage contours for a cavity radius $R = 0.6$ m at $t = 440$ μs for the L-E model (Fig. 12(a)) and the present damage model (Fig. 12(c)). As an added comparison, the computation using the well-known Johnson–Holmquist-Concrete (J–H-C) model [7] is also conducted and shown in Fig. 12(b). It can be seen that the L-E model is not capable of predicting damage at all. The J–H-C model is capable of evaluating the compression damage near the upper surface [20], but is incompetent to calculate the tensile damage. It is noted

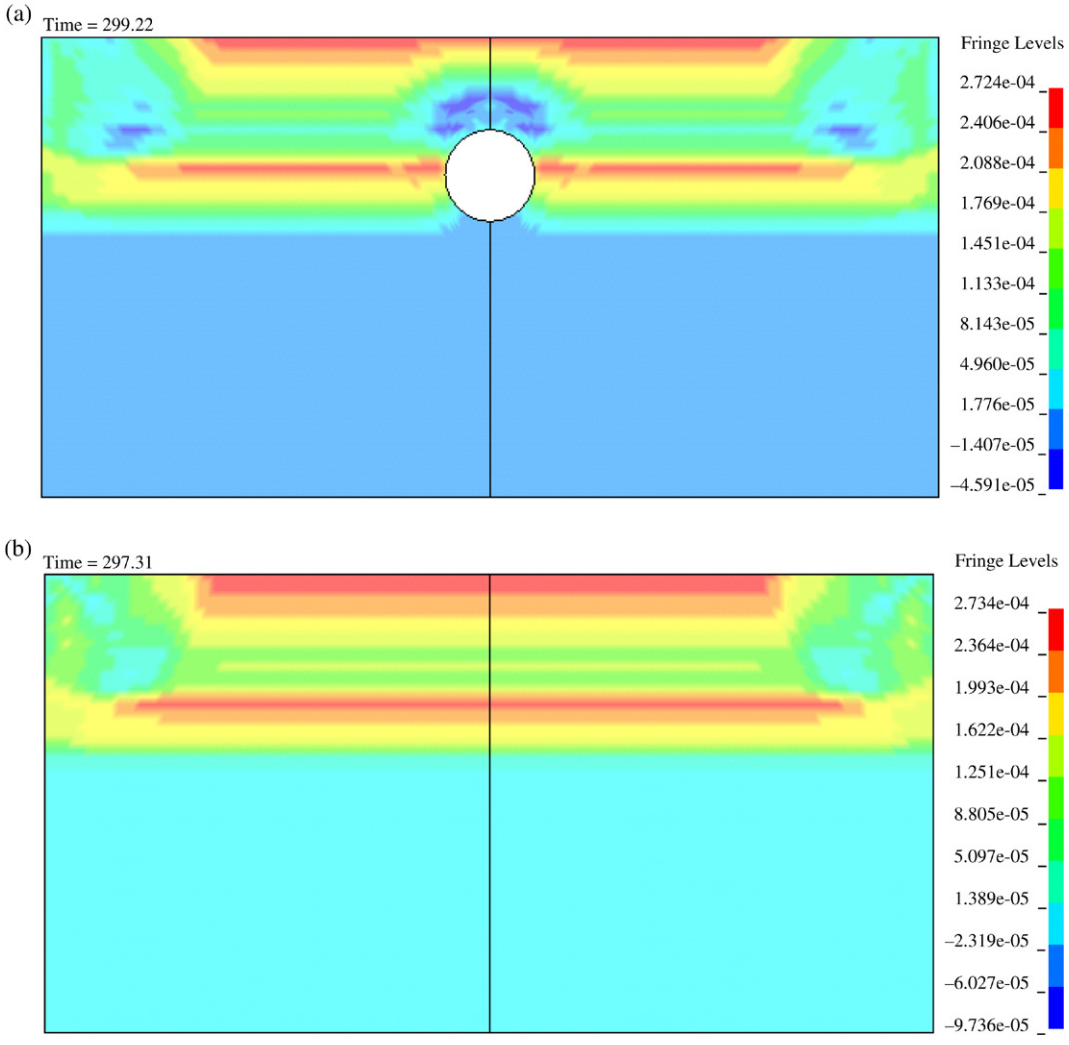


Fig. 11. Contours of hydrostatic pressure for the case (a) with cavity ($R = 0.3$ m and $e = 0.6$ m); and (b) without cavity (unit: Mbar. 1 Mbar $= 10^5$ MPa).

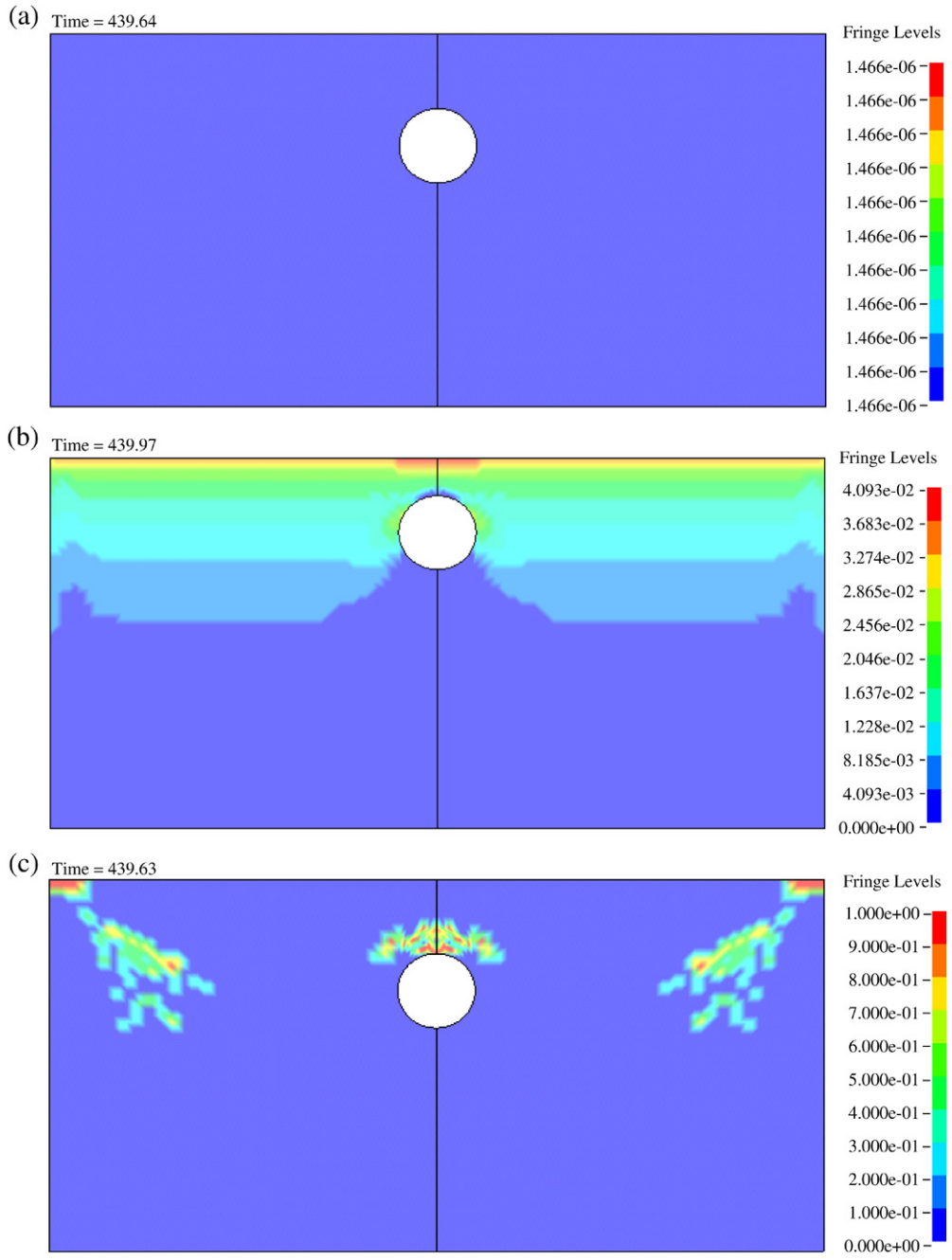


Fig. 12. Contours of damage for $R = 0.60$ m cavity at $t = 440$ μs under the same blast loading for (a) L-E model; (b) J–H-C model; and (c) continuum damage model.

that the proposed damage model used in the present study can well evaluate the tensile damage above the cavity and near the side boundaries. In particular, the spalling at those places may occur with the increase of reflected wave's magnitude. Hence, special protective measures at these identified locations are highly desirable when the applied blast loading is very large.

### 4.4. Effect of cavity position

The effect of the cavity position $e$ on the attenuation of pressure waves is shown in Fig. 13. When $R$ is fixed, the decay factors $DF$ are practically identical for all $e$ values. This phenomenon can also be observed from the time–hydrostatic pressure curves at $y = 0.5$ m shown in Fig. 14. The peak value of hydrostatic pressure does not vary much for all $e$ values. These numerical results reveal that the overhead cover of the cavity in the stress distribution layer may not be a critical factor in the design considerations of a concrete defense layer.

## 5. Empirical formula for decay factor

Based on the above numerical results, it is established that $DF$ is essentially a function of $R$ and $y$:

$$DF = f(R, y) \tag{19}$$

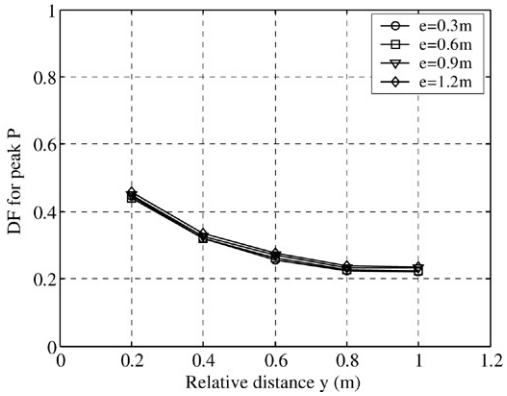


Fig. 13. Variation of decay factors for peak hydrostatic pressure with different positions $e$ of cavity.

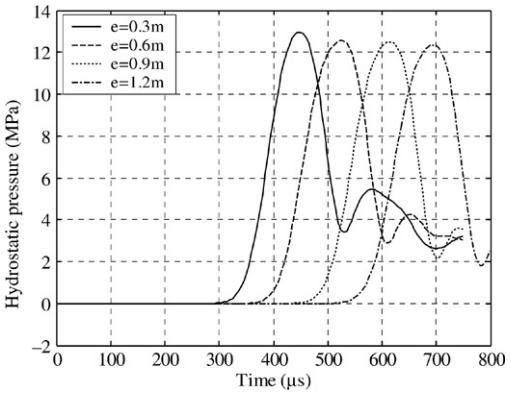


Fig. 14. Effect of cavity position $e$ on hydrostatic pressure history at $y = 0.5$ m point on $Y$-axis.

where the relative distance $y = Y - 2R - e$.

In order to determine the particular form of Eq. (19), one value of $e$ (0.30 m), four values of $R$ (0.15, 0.30, 0.45 and 0.60 m) and five values of $y$ (0.20, 0.40, 0.60, 0.80 and 1.0 m) are chosen from Fig. 10. Through a curve fitting regression analysis, $DF$ for the peak $P$ at a specified point on the $Y$-axis is approximately expressed as follows:

$$DF = \exp\left(-\sqrt{\frac{y}{R}}\right). \tag{20}$$

This formula shows that $DF$ increases with $R$ and decreases with $y$. When the term $\frac{y}{R}$ approaches zero, $DF$ is almost equal to unity. Fig. 15 shows the comparison of numerical results with the predictions from the above empirical formula. It is clear that this empirical formula agrees favorably well with the numerical results. Therefore, Eq. (20) provides a very useful and practical means to expeditiously estimate the required size of a circular cavity if the expected $DF$ (at a relative distance $y$) and position $e$ are known. On the other hand, when $DF$ and $R$ are given, the relative distance $y$ can also be determined readily from Eq. (20).

## 6. Conclusions

A numerical scheme encompassing a developed FEM subroutine for the continuum damage concrete model was established in the present study and calibrated against field blast tests. The established numerical tool was then used for further investigation of the tensile damage and attenuation effect of concrete defense layer on blast stress waves. From these studies, the following conclusions and understandings can be drawn.

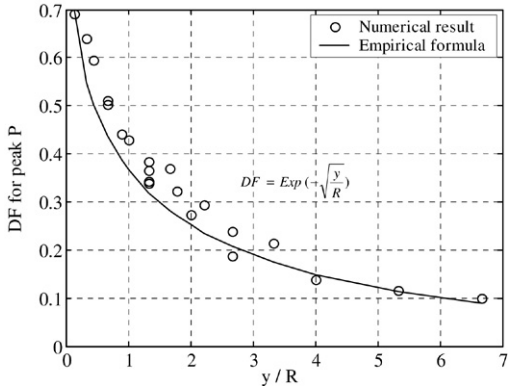


Fig. 15. Comparison of empirical formulae and numerical results of decay factors for the peak hydrostatic pressure.

(1) Compared to other models like the L-E model or J–H-C model, the continuum damage concrete model presented in this study can not only capture the tensile damage, but can also evaluate the material plastic behaviors during compression. The present numerical scheme incorporating this damage model possesses great potential and advantage for future analyses and design of perforated concrete defense layer against blast-induced stress waves.
(2) Artificial cavities embedded in the concrete defense layer have a vital effect on the attenuation of stress-waves. As for a circular cavity, the radius $R$ has a significant effect on the reduction of stress-waves according to our computations, while the effect of the position of the cavity is found to be negligible.
(3) One empirical formula is obtained to correlate the decay factor, dimensions of a circular cavity and relative distance. The formula can be employed to determine the minimum radius of a cavity $R_{\min}$, or minimum safe distance $y_{\min}$ when the decay factor is given. Therefore, it can serve as a very practical and handy tool in the process of designing an intelligent defense layer in civil defense engineering.

It should be noted that the third conclusion is applicable only when the damage of concrete does not initiate the collapse of the cavity. Further work is necessary when the damage of concrete defense layer is severe enough to cause a complete collapse of the cavity.

## Acknowledgements

The work reported herein was partially supported by the Post-doctoral Science Foundation of China (project No. 2004036468). The authors also wish to express their thanks to *The Third Institute of PLA Engineer* and *Yangtze Science Research Institute* for offering good experimental and calculational conditions.

## References


[1] Balandin DV, Bolotnik NN, Pilkey WD. Optimal protection from impact, shock, and vibration. Gordon and Breach Science Publisher; 2001.

[2] Bulson PS. Explosive loading of engineering structures. E & FN Spon Press; 1997.

[3] Dancygier AN, Yankelevsky DZ, Baum H. Behavior of reinforced concrete walls with internal plaster coating under exterior hard projectile impact. ACI Materials Journal 1999;91(1):116–25.

[4] Dowding CH. Construction vibrations. Upper Saddle River (NJ): Prentice Hall; 1996.

[5] Guruprasad S, Mukherjee A. Layered sacrificial claddings under blast loading, Part I—analytical studies. International Journal of Impact Engineering 2000;24(9):957–73.

[6] Hallquist JO. LS-DYNA theoretical manual. California (USA); 1998.

[7] Holmquist TJ, Johnson GR, Cook WH. A computational constitutive model for concrete subjected to large strains, high strain rates, and high pressures. In: Proc. 14th int. symp. on ballistics. 1993. p. 591–600.

[8] Jaeger JC, Cook NGW. Fundamentals of rock mechanics. 2nd ed. London: Chapman and Hall; 1979.

[9] Kennedey RP. Review of procedures for the analysis and design of concrete structures to resist missile impact effects. Nuclear Engineering 1976;37(2):183–203.

[10] Kinney GF, Graham KJ. Explosive shocks in air. New York: Springer; 1985.

[11] Langheim H, Pahl H, Schmolinske E, Alois S. Subscale penetration tests with bomb-advanced penetration against hardened structures. In: The 6th international symposium interaction of non-nuclear munitions with structure. 1993.

[12] Li YC, Wang XJ, Hu XZ et al. Study on layered design and its defending function. Technical report of national defense engineering. China: USTC; 2004. p. 1–55.

[13] Liu LQ, Katsabanis PD. Development of a continuum damage model for blasting analysis. International Journal of Rock Mechanics and Mining Science 1997;34(2):217–31.

[14] Livermore Software Technology Corporation (LSTC). LS-DYNA keyword user's manual. California (USA); 2003.

[15] Owen DRJ, Hinton E. Finite elements in plasticity: Theory and practice. Swansea (UK): Pineridge Press; 1980.

[16] Philippidis TP, Aggelis TG. Experimental study of wave dispersion and attenuation in concrete. Ultrasonics 2005;43(7):584–95.

[17] Robinson DN. A displacement bound principle for elastic–plastic structures subjected to blast loading. Journal of the Mechanics and Physics of Solids 1970;18(1):65–80.

[18] Rohani B. Shielding methodology for conventional kinetic energy weapons. Technical report SL-8f-8. US Army engineers Corps, Waterways Experimental Station, Vicksburg (MS); 1987, p. 23–46.

[19] Wang ZL, Li YC. Study on diffracting and screening effects of cavities on axial stress waves in defense layer. Rock and Soil Mechanics 2005;26(8): 1221–6.

[20] Wang ZL, Wang JG, Li YC, Leung CF. Attenuation effect of artificial cavity on air-blast waves in an intelligent defense layer. Computers and Geotechnics 2006;33(2):132–41.

[21] Yang R, Bawden WF, Katsabanis PD. A new constitutive model for blast damage. International Journal of Rock Mechanics & Mining Sciences 1996;33(3):245–54.

[22] Yang Z. Finite element simulation of response of buried shelters to blast loadings. Finite Elements in Analysis and Design 1997;24(3):113–32.